AGU PUBLICATIONS

JGR

Journal of Geophysical Research: Solid Earth

RESEARCH ARTICLE
10.1002/2017JB014363

Key Points:
- Iron-bearing rhyolitic and basaltic glasses exhibit distinct trends in quadrupole splittings and isomer shifts with increasing pressure
- Quadrupole splitting is affected by the composition of the silicate glasses, particularly sensitive to (K_2O + Na_2O)/FeO and (CaO + MgO)/FeO
- Rhyolitic and basaltic glasses remain in the high-spin state up to at least ~120 and 100 GPa, respectively

Supporting Information:
- Supporting Information S1

Correspondence to:
N. V. Solomatova,
nsolomat@caltech.edu

Citation:
Solomatova, N. V., J. M. Jackson, W. Sturhahn, G. R. Rossman, and M. Roskosz (2017), Electronic environments of ferrous iron in rhyolitic and basaltic glasses at high pressure, *J. Geophys. Res. Solid Earth*, *122*, 6306–6322, doi:10.1002/2017JB014363.

Received 22 APR 2017
Accepted 9 AUG 2017
Accepted article online 14 AUG 2017
Published online 31 AUG 2017

Electronic environments of ferrous iron in rhyolitic and basaltic glasses at high pressure

Natalia V. Solomatova[1], Jennifer M. Jackson[1], Wolfgang Sturhahn[1], George R. Rossman[1], and Mathieu Roskosz[2]

[1]Division of Geological and Planetary Sciences, Caltech, Pasadena, California, USA, [2]IMPMC-Muséum National d'Histoire Naturelle-CNRS, Paris, France

Abstract The physical properties of silicate melts within Earth's mantle affect the chemical and thermal evolution of its interior. Chemistry and coordination environments affect such properties. We have measured the hyperfine parameters of iron-bearing rhyolitic and basaltic glasses up to ~120 GPa and ~100 GPa, respectively, in a neon pressure medium using time domain synchrotron Mössbauer spectroscopy. The spectra for rhyolitic and basaltic glasses are well explained by three high-spin Fe^{2+}-like sites with distinct quadrupole splittings. Absence of detectable ferric iron was confirmed with optical absorption spectroscopy. The sites with relatively high and intermediate quadrupole splittings are likely a result of fivefold and sixfold coordination environments of ferrous iron that transition to higher coordination with increasing pressure. The ferrous site with a relatively low quadrupole splitting and isomer shift at low pressures may be related to a fourfold or a second fivefold ferrous iron site, which transitions to higher coordination in basaltic glass, but likely remains in low coordination in rhyolitic glass. These results indicate that iron experiences changes in its coordination environment with increasing pressure without undergoing a high-spin to low-spin transition. We compare our results to the hyperfine parameters of silicate glasses of different compositions. With the assumption that coordination environments in silicate glasses may serve as a good indicator for those in a melt, this study suggests that ferrous iron in chemically complex silicate melts likely exists in a high-spin state throughout most of Earth's mantle.

1. Introduction

Iron-bearing silicate melts may exist in the lower mantle, particularly near the core-mantle boundary [*Williams and Garnero*, 1996; *Vidale and Hedlin*, 1998; *Maruyama et al.*, 2007; *Thomas et al.*, 2012]. The behavior of iron in melts derived from mantle rocks is poorly understood but in some cases may be approximated by iron-bearing glasses. The local structure environment around iron in a glass can be taken as a good approximation for the melt structure, provided the quench rates are fast enough through the temperature interval of the glass transition, T_g [e.g., *Rossano et al.*, 2008; *Wilke et al.*, 2007]. Using X-ray absorption spectroscopy at the iron K-edge, *Wilke et al.* [2007] use the integrated pre-edge intensity and centroid position to determine iron's average coordination in Na-, K-, and Al-bearing silicate melts and glasses. The average coordination of Fe^{2+} is found to be close to five, with a slightly higher concentration of fourfold coordinated Fe^{2+} in the melts compared to glasses. There is most likely a distribution of site geometries in the glasses. When compared to the liquid, the short-range metal-anion interatomic distances of quenched glasses have been shown to be similar or slightly shorter and the next-nearest neighbor distances longer, while the average coordination numbers of cations are smaller in the liquid (glass) than the crystalline aggregate. During crystallization, partitioning of the cations likely takes place between fourfold, fivefold, and sixfold coordination sites in the liquid and the octahedral sites in a crystal [*Burns*, 1993].

Nevertheless, previous studies have conflicting conclusions on the coordination of iron in silicate glasses, especially at high pressures. Experiments using X-ray absorption near edge spectroscopy on mid-oceanic ridge basalt (MORB) glasses have revealed that the average coordination of iron is about five regardless of oxidation state and may potentially be a mixture of fourfold, fivefold, and sixfold coordinated iron [*Wilke et al.*, 2005]. *Guo et al.* [2013] conducted high-temperature density measurements on CaO-FeO-SiO_2 melts with 40 mol % FeO, finding a positive correlation between polymerization and the coordination of ferrous iron. The average coordination ranged from 4.6 to 5.2, consistent with studies using X-ray absorption near edge spectroscopy [*Farges et al.*, 2005; *Jackson et al.*, 2005; *Wilke et al.*, 2005, 2007]. Nevertheless, it is still challenging to correlate spectral features to coordination environments in

Table 1. Oxide Weight Percents of Silicate Glasses Considered in This Study[a]

	MgO %	FeO %	Fe_2O_3%	CaO %	Na_2O %	K_2O %	TiO_2%	Al_2O_3%	SiO_2%
Basaltic glass	18.33	7.61	-	11.40	1.03	0.09	0.86	14.46	46.26
Rhyolitic glass	0.05	4.10	-	0.03	4.54	4.49	0.00	10.44	75.71
Andesitic glass	8.30	7.04	-	7.22	2.98	1.44	0.81	16.30	55.80
Dacitic glass	4.23	4.47	-	4.68	3.93	2.50	0.71	14.90	64.10
Murakami et al. [2014]	30.16	13.63	-	0.00	0.00	0.00	0.00	0.00	56.20
Gu et al. [2012], Al free	30.16	13.63	-	0.00	0.00	0.00	0.00	0.00	56.20
Gu et al. [2012], Al bearing	28.26	13.62	-	0.00	0.00	0.00	0.00	4.77	53.35
Mao et al. [2014]	31.05	1.56	6.15	0.00	0.00	0.00	0.00	4.97	56.26
Prescher et al. [2014], Fe^{3+} free	31.62	9.38	-	0.00	0.00	0.00	0.00	2.77	56.24
Prescher et al. [2014], Fe^{3+} bearing	0.00	9.29	25.44	0.00	12.91	0.00	0.00	0.00	52.36
Alberto et al. [1996], sample A	0.00	5.00	-	34.1	0.00	0.00	0.00	0.00	60.9
Rossano et al. [1999], Thailand tektite	2.02	4.91	0.29	2.23	1.21	2.16	0.77	12.73	73.27
Dorfman et al. [2016]	0.00	33.56	7.63	0.00	0.00	0.00	0.00	22.50	36.31
Jackson et al. [2005], BAS	0.00	13.74	-	9.96	3.07	0.00	0.00	15.85	50.08
Jackson et al. [2005], NC2	0.00	17.22	-	9.52	11.25	0.00	0.00	0.00	62.01
Jackson et al. [2005], NA1	0.00	27.51	-	0.00	10.95	0.00	0.00	0.00	61.54

[a]The Fe_2O_3 % is estimated as 0 for reduced glasses with Fe^{3+} content below the detection level of the fit, except for *Rossano et al.* [1999] where coulometric titration was used to determine the exact Fe^{3+} content. The rhyolitic and basaltic glasses contain about 0.02–0.04 wt % and 0.005–0.008 wt % of OH^-, respectively (see text for details). The tektite in *Rossano et al.* [1999] has 0.03 wt % P_2O_5.

glasses, in part due to the range and distribution of available coordination environments. In Mössbauer experiments conducted in the energy domain, the spectra are often fit using correlated distributions to capture these phenomena in glasses, yet challenges still remain. Conventional Mössbauer experiments have reported fivefold coordinated Fe^{2+} with small amounts of fourfold and sixfold coordinated Fe^{2+} for a suite of natural MORB glasses [*Cottrell and Kelley*, 2011], as well as predominantly sixfold Fe^{2+} with small amounts of fourfold Fe^{2+} in natural tektites and synthetic CaO-SiO_2-FeO glasses [*Alberto et al.*, 1996; *Rossano et al.*, 1999]. Spectra from time domain synchrotron Mössbauer experiments at high pressures have been fit with one to three Fe^{2+} sites with a wide range of quadrupole splitting and isomer shift values, but without the use of correlated distributions. These data sets have been used to interpret a range of spin, and in some cases oxidation states for the iron cations, leading to conflicting predictions on whether iron in lower mantle silicate melts goes through a high-spin to low-spin transition [*Nomura et al.*, 2011; *Gu et al.*, 2012; *Murakami et al.*, 2014]. *Ramo and Stixrude* [2014] used first-principle molecular dynamics to study the spin crossover of iron in liquid Fe_2SiO_4. Their PBE + U calculations at 3000 K indicate that the magnetic moment of iron remains close to the initial magnetic moment of ~3.7 μ_B throughout the majority of the lower mantle and that the spin transition region is expected to be very broad (>200 GPa). Additional studies are necessary to help constrain the geometric and electronic state of iron in silicate melts and glasses at high pressure.

2. Methods

2.1. Sample Preparation

The silicate glasses were synthesized at the University of Lille, France, from powdered mixtures of SiO_2, Al_2O_3, $CaCO_3$, MgO, Na_2CO_3, K_2CO_3, TiO_2, and Fe_2O_3, which were melted at 1550°C and rapidly quenched in air after 2–3 h in the furnace. The oxidation state of iron was equilibrated with the imposed oxygen fugacity, log(fO_2) of −8 (iron-wüstite buffer, IW + 0.3) using CO/CO_2 gas mixtures. For more synthesis details, we refer the reader to *Dauphas et al.* [2014]. The compositions of the glasses were determined with an electron microprobe at the UMET laboratory in the University of Lille 1. The oxide weight percents for the rhyolitic and basaltic glasses are listed in Table 1, and the oxide mole percents are illustrated in Figure 1.

Two diamond anvil cells with beveled 250 μm diamonds on tungsten-carbide seats were assembled for the high-pressure measurements. For each experiment, a rhenium gasket of ~50 μm thickness was prepared by drilling a hole with a ~ 90 μm diameter. In one diamond anvil cell, a 60 by 50 μm chip of rhyolitic glass with a thickness of about 11 μm was loaded onto the center of the diamond culet and two ruby spheres with diameters of 6 and 7.5 μm, respectively, were loaded next to the sample as a pressure gauge. In the

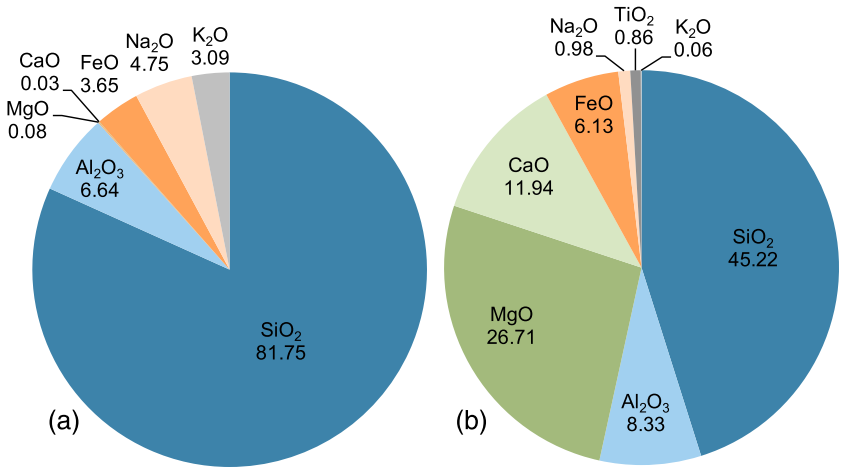

Figure 1. Composition in oxide mole percents for (a) rhyolitic glass and (b) basaltic glass. The rhyolitic and basaltic glasses contain about 0.1–0.2 mol % and 0.03–0.05 mol % of OH^-, respectively (see text for details).

second diamond anvil cell, a ~ 40 μm chip of basaltic glass with a thickness of about 12 μm was loaded with a 10 μm ruby sphere. Both cells were loaded with neon at 25000 psi using the gas-loading system at Caltech.

2.2. Experimental Methods

Optical absorption spectroscopic measurements were conducted on polished samples of the rhyolitic and basaltic glasses with thicknesses of 95 and 300 μm, respectively, at room temperature. Room temperature ultraviolet/visible/near-infrared (UV/VIS/NIR) absorption spectra were collected at the Caltech mineral spectroscopy laboratory in the wave number range of ~27100 cm^{-1} and 2000 cm^{-1} for the rhyolitic glass and ~27700 cm^{-1} and 1200 cm^{-1} for the basaltic glass. For wave numbers below about 10000 cm^{-1}, we used a Nicolet iS50 FT-IR spectrometer with CaF_2, KBr, and SiO_2 beamsplitters and InGaAs and deuterated triglycine sulfate detectors. Above 10000 cm^{-1}, we used a Si diode array spectrometer. The sample chamber of the Nicolet iS50 FT-IR spectrometer was purged to reduce atmospheric H_2O and CO_2 in the infrared region. Spectra were averaged over approximately 1000–2000 scans in the UV/VIS region and 200–400 scans in the IR region.

Relevant hyperfine parameters for the silicate glasses were determined with Mössbauer spectroscopy [*Mössbauer*, 1962]. The isomer shift (IS) originates from the electron density at the nucleus and is indirectly influenced, via shielding effects, by the *d* electrons in the valence shell, thus allowing constraints on the oxidation state. A nuclear quadrupole splitting (QS) results from a nonvanishing electric field gradient at the Mössbauer nucleus occupying a state with an angular momentum quantum number $I > 1/2$. The QS yields information on the local coordination environment, and complementary to the isomer shift, oxidation and spin states of the atom can be deduced.

Conventional energy domain ^{57}Fe Mössbauer spectroscopic experiments were conducted using a radioactive source at 1 bar and 298 K. The spectra for the basaltic and andesitic glasses were collected at the Advanced Photon Source (APS), and the spectra for rhyolitic and dacitic glasses were collected at the Unité Matériaux et Transformations (UMET) laboratory. High-pressure hyperfine parameters for the rhyolitic and basaltic glasses were determined with time domain synchrotron Mössbauer spectroscopy (SMS). The SMS measurements were conducted at Sector 3-ID-B of the APS. The storage ring was operated in top-up mode with 24 bunches separated by 153 ns. A high-resolution monochromator was tuned to the 14.4125 keV nuclear transition energy of ^{57}Fe with a full width at half maximum (FWHM) of 1 meV [*Toellner*, 2000]. The beam was focused to an area of 10 by 11 μm^2 using a Kirkpatrick-Baez mirror system [*Zhang et al.*, 2015]. The time spectra were measured with an avalanche photodiode detector, positioned ~0.5 m downstream from the sample in the forward direction. A time window of 21 to 128 ns after excitation was used to observe nuclear resonant scattering and fit the data.

A stainless steel (SS) foil was placed in the downstream direction as a reference absorber for isomer shift measurements. At each compression point, an SMS spectrum was collected for the sample with and without a naturally ^{57}Fe-enriched SS foil. For the experiments on rhyolitic glass, a 25 μm SS foil was used between 3.2 and 25.3 GPa, a 6 μm SS foil was used between 31.2 and 94.0 GPa, and a 10 μm SS foil was used between 102 and 119 GPa. For the experiments on basaltic glass, we used a 10 μm SS foil for the entire pressure range. The isomer shifts between the SS foils and α-iron metal were measured at the APS using a radioactive source and found to be −0.107(4), −0.100(3), and −0.094(3) mm/s with a corresponding FWHM (due to the combined effect of site distribution and source broadening) of 0.42(1), 0.445(9), and 0.50(1) mm/s for the 6, 10, and 25 μm SS foils, respectively. Pressure was determined before and after the SMS data collection with ruby fluorescence at GSECARS of the APS using the ruby fluorescence pressure scale reported in *Dewaele et al*. [2008]. *Gu et al*., [2012], *Mao et al*. [2014], *Prescher et al*., [2014], and *Dorfman et al*., [2016] used the ruby pressure scale reported in *Mao et al*. [1986], which underestimates the pressure (e.g., by about 2 GPa at 60 GPa). The average pressure drifts during the measurements were 0.3 GPa for the rhyolitic glass and 0.6 GPa for the basaltic glass. For the rhyolitic glass, pressure was measured with the first-order Raman band of the diamond anvils above 94 GPa [*Akahama and Kawamura*, 2006]. We assume a pressure error of 3 GPa above 94 GPa, accounting for the systematic difference between Raman band pressure and ruby pressure.

2.3. Fitting Procedure of Mössbauer Spectra

Synchrotron Mössbauer spectroscopy spectra were fitted with version 2.1.1 of the CONUSS software [*Sturhahn*, 2000], which uses a least square algorithm to fit iron's hyperfine parameters (e.g., isomer shift, quadrupole splitting, and distribution of the quadrupole splitting expressed as the full width at half maximum, and the correlation parameter for the distributions), sample thickness, and relative weights of the sites. We used the dual fit module within the CONUSS software (implemented in version 2.1.1), which fits the spectrum of the sample and sample with SS simultaneously and permits the use of prior information ("priors") in fitting of the data. It is important to use a well-defined reference foil with a uniform effective thickness that is similar to that of the sample. For evaluations of data of the rhyolitic glass sample between 3.2 and 25.3 GPa, the relatively large effective thickness of the 25 μm stainless steel foil required a prior of 1.08 mm/s with a prior window of ±0.01 mm/s for the isomer shift of site 1 (equivalent to the isomer shift of site 2) and a prior of 0.80 mm/s with a prior window of ±0.01 mm/s for the isomer shift of site 3. Prior values correspond to the isomer shifts of the two sites fitted in the ambient pressure spectra that were collected using a radioactive source, adjusted relative to the 25 μm thick stainless steel foil. No priors were used for pressures above 25.3 GPa, and no priors were used while fitting the spectra of the basaltic glass.

Energy domain Mössbauer absorption spectra of silicate glasses are typically composed of asymmetrical doublets due to site distributions. To account for the spectral asymmetry, we model the distributions of the isomer shift and quadrupole splitting as linearly correlated. The use of correlated isomer shift and quadrupole splitting distributions result in a lower reduced χ^2 compared to models without the use of correlated distributions. In CONUSS, one-dimensional distributions are implemented with the possibility to attach a second parameter corresponding to a pseudo two-dimensional distribution defined by the covariance matrix

$$\hat{\sigma} = \frac{\mathrm{FWHM}^2}{8\ln 2}\begin{pmatrix} 1 & \Delta \\ \Delta & \Delta^2 \end{pmatrix},$$

where Δ is the attachment parameter. The distribution width of the two lines is then

$$\mathrm{FWHM}_{\pm} = \left|1 \pm \frac{\Delta}{2}\right| \mathrm{FWHM}.$$

Two values of Δ and FWHM

$$\Delta_1 = 2\frac{\mathrm{FWHM}_+ + \mathrm{FWHM}_-}{\mathrm{FWHM}_+ - \mathrm{FWHM}_-}$$

$$\Delta_2 = 2\frac{\mathrm{FWHM}_+ - \mathrm{FWHM}_-}{\mathrm{FWHM}_+ + \mathrm{FWHM}_-}$$

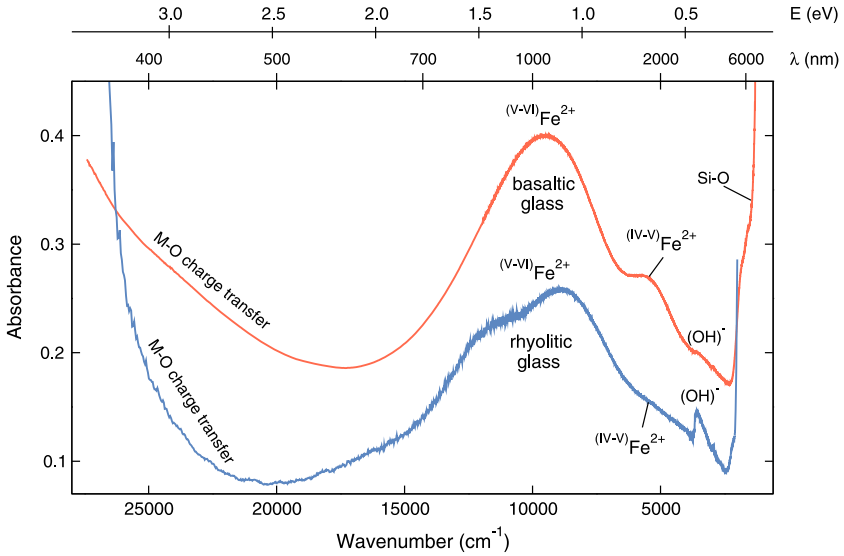

Figure 2. UV/VIS/NIR absorption spectra of rhyolitic glass (blue) and basaltic glass (red). The samples were polished to a thickness of 95 and 300 μm, respectively. The spectra are plotted for an equivalent iron concentration, and offset for clarity.

$$\mathrm{FWHM}_1 = \frac{1}{2}|\mathrm{FWHM}_+ - \mathrm{FWHM}_-|$$

$$\mathrm{FWHM}_2 = \frac{1}{2}|\mathrm{FWHM}_+ + \mathrm{FWHM}_-|$$

lead to identical spectra. Thus, one may obtain alternative solutions using the relationship: $\Delta_2 = 4/\Delta_1$ and $\mathrm{FWHM}_2 = 2\mathrm{FWHM}_1/\Delta_2$. For example, for site 1 in basaltic glass at 60.5 GPa, the FWHM is 0.68 mm/s and the attachment parameter is 0.27; the alternative solution is a FWHM of 0.09 mm/s and an attachment parameter of 14.65. We choose the FWHM similar to those reported in high-pressure energy domain synchrotron Mössbauer studies on silicate glasses [*Murakami et al.*, 2014; *Prescher et al.*, 2014; *Dorfman et al.*, 2016].

3. Results

3.1. Optical Absorption Spectroscopy

The ultraviolet/visible/near-infrared (UV/VIS/NIR) absorption spectra of rhyolitic and basaltic glasses are shown in Figure 2. The dominant features of the spectrum of rhyolitic glass are two intense bands at ~9000 cm^{-1} and 12500 cm^{-1}, while the dominant feature of the spectrum of basaltic is an intense absorption band near ~9500 cm^{-1}. The spectrum of the basaltic glass also has an absorption band at ~5000 cm^{-1}, which appears as a shoulder in the spectrum of the rhyolitic glass. These absorption bands are consistent with electronic transitions in ferrous iron in fourfold, fivefold, and/or sixfold coordination in silicate glasses [e.g., *Boon and Fyfe*, 1972; *Iwamoto et al.*, 1978; *Nolet*, 1980; *Jackson et al.*, 2005; *Kido et al.*, 2006; *Carl et al.*, 2007; *Rossano et al.*, 2008; *Klement et al.*, 2009]. Distorted octahedral ferrous sites (e.g., the M2 crystallographic site in orthopyroxenes) result in absorption bands at about 11000, 5400, and 2350 cm^{-1} [*Goldman and Rossman*, 1977]; fivefold ferrous iron sites in grandidierite and joaquinite result in two to three absorption bands between 12550 and 9500 cm^{-1} and one at around 4500–5000 cm^{-1} [*Rossman and Taran*, 2001]; and tetrahedral ferrous sites typically result in absorption bands between 2500 and 6250 cm^{-1} [*Burns*, 1985; *Rossman and Taran*, 2001]. In a glass, iron atoms most likely occupy a continuum of coordination environments. Nonetheless, a qualitative assessment of the optical spectra suggests that there is a low concentration of tetrahedrally coordinated iron in these glasses. In the basaltic glass, the approximate fourfold ferrous iron concentration with respect to total ferrous iron is 0.6–14%, assuming that the 5000 and 9500 cm^{-1} bands are entirely due to fourfold and sixfold ferrous iron with a molar extinction coefficient of 30–40 L/mol cm and 1–16 L/mol cm, respectively [*Rossman and Taran*, 2001; *Klement et al.*, 2009]. The rhyolitic glass contains about half the concentration of tetrahedrally coordinated iron compared to the basaltic glass using the same

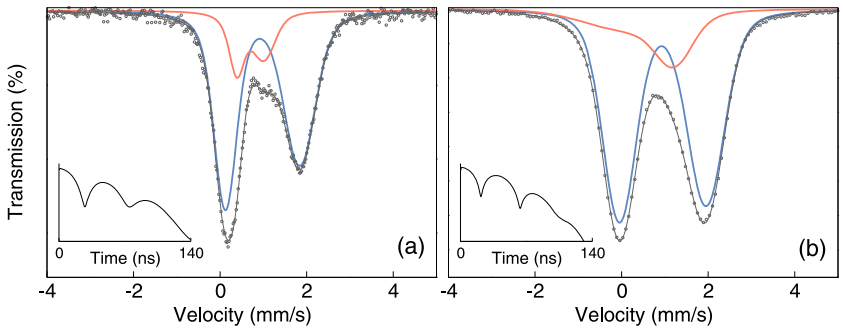

Figure 3. Conventional Mössbauer spectra for (a) rhyolitic glass and (b) basaltic glass at room pressure and temperature, and the corresponding best fits. Blue and red lines correspond to site 1 and site 2, respectively. Insets show modeled time domain spectra of these best fits.

assumptions. Thus, the majority of the iron in the rhyolitic and basaltic glasses most likely exist in fivefold and/or distorted sixfold coordination, similar to that reported in the *Jackson et al.* [2005] study for iron-bearing silicate glasses of a wide variety of compositions (see Table 1).

There are no clearly identifiable Fe^{3+} features in the optical absorption spectra; however, small amounts of Fe^{3+} cannot be excluded based on these spectra due to the intense metal-oxygen charge transfer in the ultraviolet region above ~20000 cm^{-1} [*ElBatal et al.*, 2007; *Carl et al.*, 2007]. The very intense absorption band at ~950–1100 cm^{-1} is due to the Si-O fundamental stretching mode, and the less intense absorption bands at about 1600–1950 cm^{-1} evident in the basaltic glass are related to Si-O stretching overtones [*Manghnani et al.*, 1974; *Costa et al.*, 1997; *Karakassides et al.*, 1999; *Madejová and Komadel*, 2001]. In both glasses, the sharp features at about 3500 cm^{-1} are due to structural OH^-. We fitted a Gaussian function to the dominant OH^- band at 3583 and 3451 cm^{-1} in the rhyolitic and basaltic glasses, respectively. The molar extinction coefficients for the OH^- vibrational bands depend on the composition and the OH^- content of the glasses. Using values of 60 to 100 L mol^{-1} cm^{-1} as lower and upper bounds [*Newman et al.*, 1986; *Pandya et al.*, 1992; *Behrens and Stuke*, 2003], we find that the rhyolitic glass likely contains about 0.02–0.04 wt % (0.1–0.2 mol %) of OH^-, while the basaltic glass contains about 0.005–0.008 wt % (0.03–0.05 mol %) of OH^-.

3.2. Mössbauer Spectroscopy

Conventional Mössbauer spectra for the rhyolitic and basaltic glasses used in this study were reported in *Dauphas et al.* [2014], but detailed fits of the hyperfine parameters were not reported. These spectra are shown in Figure 3 with our best fits. The rhyolitic glass required two Fe^{2+}-like sites with weight fractions, 0.80(5) and 0.20 for the sites with a higher and lower QS, respectively, where the uncertainties are given in parenthesis at the 68% confidence level (Table 2). The first site is characterized by a QS of 1.729(9) mm/s and an IS of 0.982(2) mm/s. The second site is characterized by a QS of 0.65(2) mm/s and an IS of 0.705(8) mm/s. The basaltic glass required two sites with weight fractions, 0.83(6) and 0.17 for the sites with a higher and lower QS, respectively. The first site is characterized by a QS of 1.995(7) mm/s and an isomer shift of 0.948(3) mm/s, whereas the second site is characterized by a QS of 0.96(5) mm/s and an IS of 0.69(2) mm/s. For both glasses, the site with the higher QS is likely a result of fivefold and/or sixfold coordination Fe^{2+}, while the site with the lower QS can be attributed to fourfold or fivefold Fe^{2+} (see section 4 for more details). The

Table 2. Best Fit Hyperfine Parameters for Rhyolitic, Basaltic, Andesitic, and Dacitic Glasses From Fitting the Ambient Conventional Mössbauer Spectra With the CONUSS Software[a]

	Weight 1	QS Site 1 (mm/s)	IS Site 1 (mm/s)	FWHM Site 1 (mm/s)	Δ Site 1	QS Site 2 (mm/s)	IS Site 2 (mm/s)	FWHM Site 2 (mm/s)	Δ Site 2
Rhyolitic glass	0.80(5)	1.729(9)	0.982(2)	0.571(9)	0.38(2)	0.65(2)	0.705(8)	0.37(2)	0.66(9)
Basaltic glass	0.83(6)	1.995(7)	0.948(3)	0.804(6)	0.102(6)	0.96(5)	0.69(2)	1.72(6)	−1.09(7)
Andesitic glass	0.77(4)	2.032(8)	1.001(3)	0.812(7)	0.086(2)	1.00(3)	0.922(2)	1.24(7)	−0.84(5)
Dacitic glass	0.94(9)	1.859(3)	1.040(2)	0.632(5)	0.276(8)	0.70(8)	0.91(4)	0.80(8)	−1.18(9)

[a]The uncertainties are given in parentheses at the 68% confidence level for the last reported significant digit.

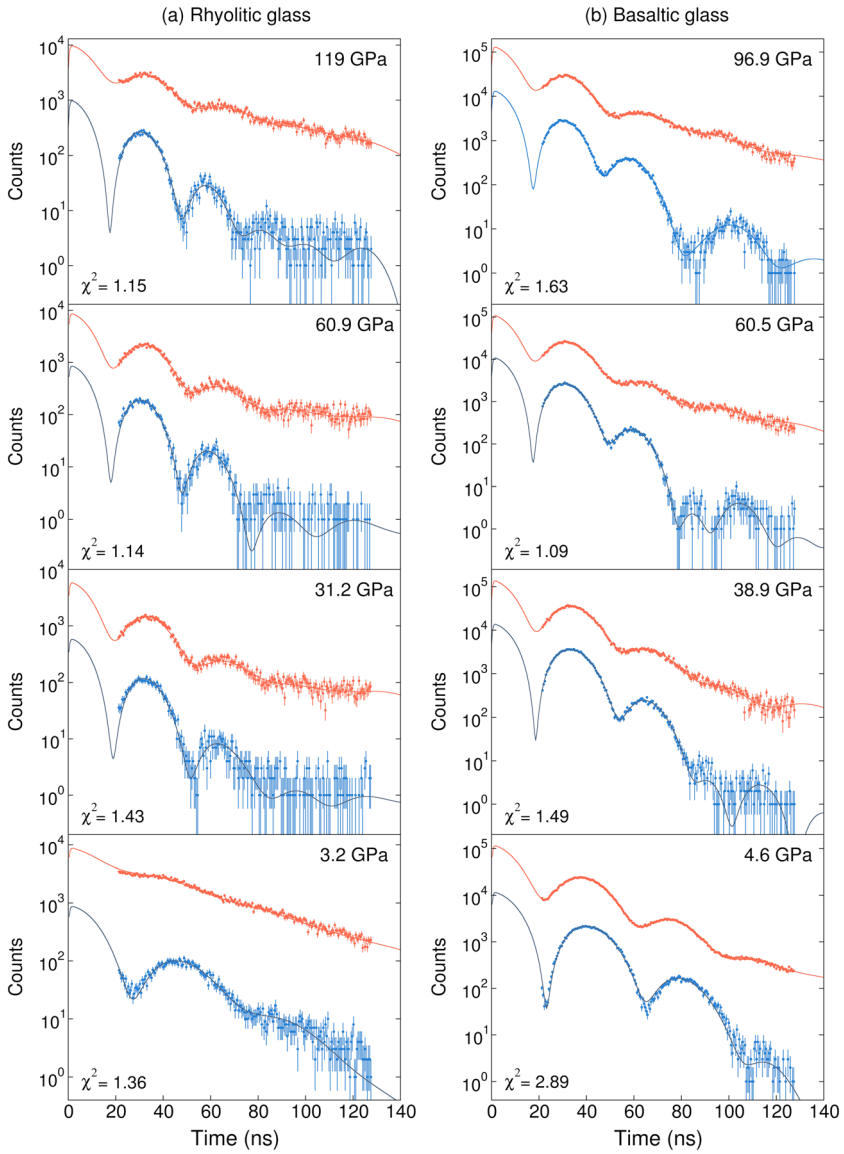

Figure 4. Select synchrotron Mössbauer spectra of (a) rhyolitic glass (Table 3) and (b) basaltic glass (Table 5) without stainless steel foil (blue) and with stainless steel foil (red) in the X-ray beam path. Their corresponding best fits with the reduced χ^2 for each dual fit are shown in the lower left corner.

spectra of basaltic glass can also be fitted with a three-site model but results in a slightly worse fit than the two-site model. Attempts were made to fit the low-pressure energy domain and time domain spectra with 5–10% Fe^{3+} (i.e., isomer shift values below about 0.5 mm/s [*Mysen*, 1987; *Burns*, 1994]); however, these models did not reproduce the shape of the spectra well and resulted in significantly higher χ^2 values. Thus, we conclude that the Fe^{3+} content in our samples is below the detection limits of Mössbauer and optical absorption spectroscopy.

Typical high-pressure time domain synchrotron Mössbauer spectra (SMS) for rhyolitic and basaltic glass are shown in Figure 4 together with their best fit models. The hyperfine parameters of the best fit models were then used to calculate the energy spectra shown in Figure 5. The spectra for rhyolitic glass required three sites with weight fractions, 0.34(2), 0.47, and 0.19 for site 1, site 2 and site 3, respectively (Figure 6). These values were determined from Monte Carlo searches and a careful analysis of χ^2, because strong parameter correlations prevented unconstrained variation. The isomer shifts for site 1 and site 2 are very similar and are constrained to be equal. The steep increase at low pressures in the QS values for site 1 plateaus at

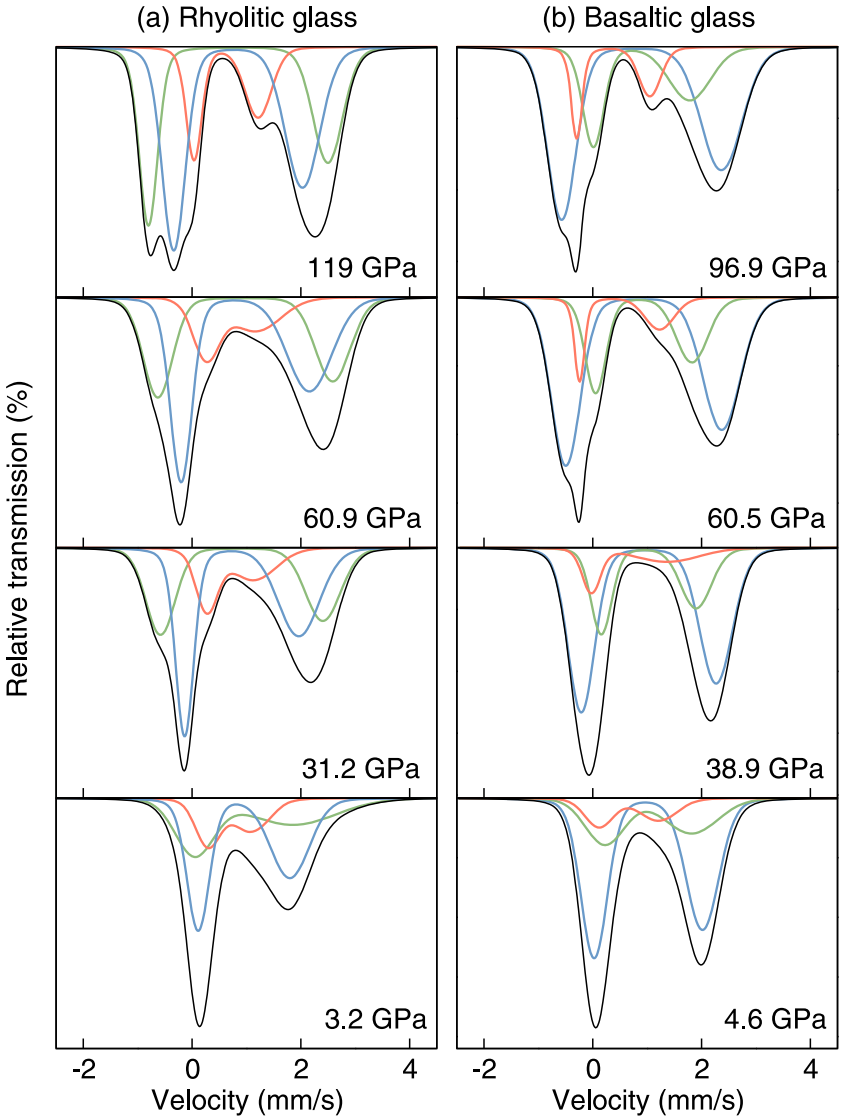

Figure 5. Modeled energy spectra of rhyolitic and basaltic glass using the best fit parameters (Tables 3 and 5, respectively). Blue, green, and red lines correspond to site 1, site 2, and site 3, depicted as blue, green, and red circles in Figure 6. Source broadening is not modeled and isomer shifts are relative to α-iron.

~3.1–3.3 mm/s above about 40 GPa. The shallow increase of the QS for site 2 up to ~50 GPa is followed by a plateau at ~2.3–2.4 mm/s. The QS of site 3 increases slowly with pressure from 0.63 mm/s at 0 GPa to 1.18 mm/s at 119 GPa. The IS values are roughly constant at about 1 and 0.7 mm/s up to 81 GPa, after which they decrease to 0.85 and 0.63 mm/s at 119 GPa for the first two sites and the third site, respectively. Hyperfine parameters for rhyolitic glass are tabulated in Table 3, and the correlation matrix for the fitted parameters at 60.9 GPa is reported in Table 4.

The SMS spectra for basaltic glass also required three sites (Figure 6). Between 1.8 and 84 GPa, the weight fractions were fixed at 0.62(3), 0.26, and 0.12 for site 1, site 2, and site 3, respectively. As in the case of the rhyolitic glass, variations of these values were accompanied by large errors caused by strong parameter correlations. Therefore, they were determined from Monte Carlo searches and a careful analysis of χ^2 and correlations between fitted parameters. There was no need to vary the weights for spectra collected at pressures higher than 84 GPa due to excellent fits to both sample and sample with the stainless steel reference absorber. At higher pressures, we found that the best weight fractions are 0.60(2), 0.26, and 0.14 for site 1, site 2, and site 3, respectively. Between 0 and 8 GPa, the QS of site 1 is constant around 2 mm/s, increases

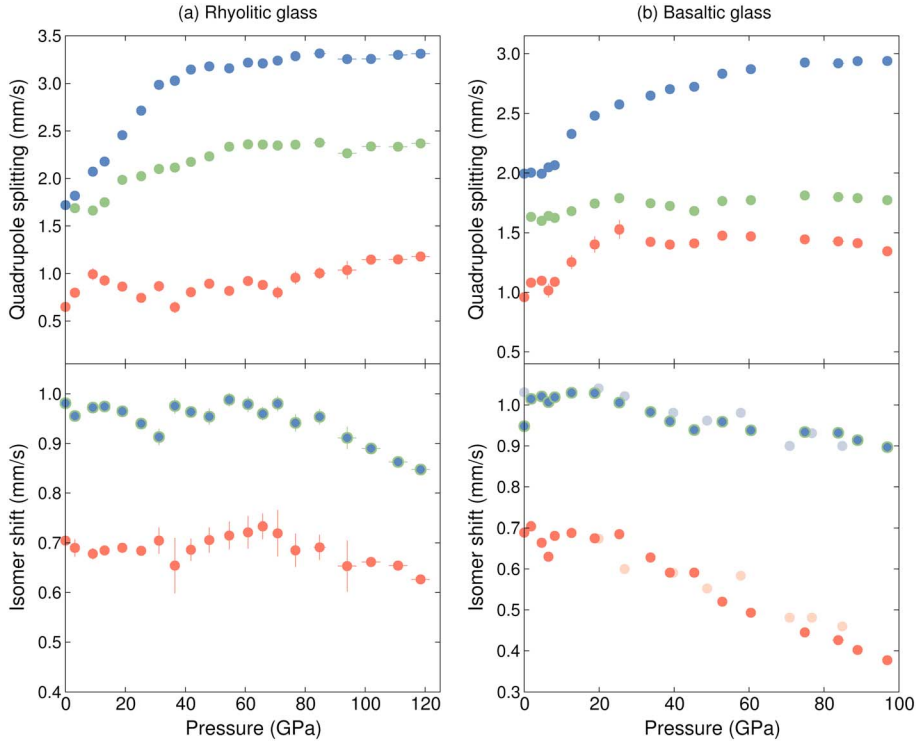

Figure 6. Quadrupole splitting and isomer shift (relative to α-Fe) of (a) rhyolitic glass and (b) basaltic glass. Blue circles correspond to Fe^{2+} with a high quadrupole splitting (site 1), green circles are Fe^{2+} with an intermediate quadrupole splitting (site 2), and red circles are Fe^{2+} with a low quadrupole splitting (site 3). The isomer shifts of site 1 and site 2 are set to be equivalent (blue circles with a green outline). Pastel circles are isomer shift values for $(Mg_{0.8}Fe_{0.2})SiO_3$ glass [*Murakami et al.*, 2014]. See section 4 for discussion. At 0 GPa, the relative weight fractions are 0.80 and 0.20 for site 1 and site 2, respectively (Figure 6a). Above 0 GPa, the relative weights are 0.34, 0.47 and 0.19 for site 1, site 2, and site 3 respectively. At 0 GPa, the relative weight fractions are 0.83 and 0.17 of the high and low QS sites, respectively (Figure 6b). Between 1.8 and 84 GPa, the relative weights are 0.62, 0.26 and 0.12 for site 1, site 2, and site 3, respectively. At 89.0 and 96.9 GPa, the relative weights are 0.6, 0.26, and 0.14 for site 1, site 2, and site 3, respectively.

with pressure from 12 to 60 GPa, after which it plateaus to ~2.9 mm/s. The QS of site 2 is roughly constant around 1.7 mm/s, while the QS of site 3 increases from 0.96 mm/s at 0 GPa to about 1.5 mm/s at 25 GPa, after which it plateaus at ~1.4 mm/s. The IS of site 1 and site 2 are constant up to 25 GPa at ~1 mm/s, after which it decreases to ~0.9 mm/s at the highest pressure, while the isomer shift of site 3 remains constant at ~0.7 mm/s up to 25 GPa after which it decreases to 0.37 mm/s at the highest pressure. The negative slope of the IS with pressure for the Fe^{2+} sites is consistent with previous studies on silicate glasses of similar composition [*Murakami et al.*, 2014; *Prescher et al.*, 2014]. Attempts were made to fit the high-pressure data with a fourth ferrous site with low-spin hyperfine parameters (QS = 0–0.4 mm/s and IS = 0.3–0.6 mm/s), but after extensive Monte Carlo searches, such a site in any proportion could not fit the data. Hyperfine parameters for basaltic glass are tabulated in Table 5, and the correlation matrix for the fitted parameters at 60.5 GPa is reported in Table 6.

4. Discussion

4.1. Coordination Environments at Room Pressure

In silicate minerals at ambient conditions, sixfold ferrous iron sites typically show QS values ranging from 1.5 to 3.2 mm/s and IS values of 1 to 1.2 mm/s. For eightfold ferrous iron sites, QS values of 3.2 to 3.5 mm/s and IS values of 1.2 to 1.3 mm/s have been observed [e.g., *Burns* 1994; *Dyar et al.*, 2006]. The range of QS values for sixfold ferrous iron has been correlated to the degree of distortion of the local site environment [*Burns*, 1994; *Victor et al.*, 2001; *Dyar et al.*, 2006; *Zhang et al.*, 2011].

The range of reported QS and IS values of fourfold ferrous iron is shifted to lower values, with some overlap, relative to those of sixfold coordinated sites. QS values range from 0.7 to 2.3 mm/s with IS values of about 0.9

Table 3. Best Fit Hyperfine Parameters for Rhyolitic Glass and the Corresponding Reduced χ^2 From Fitting the Time Domain Synchrotron Mössbauer Spectra With the CONUSS Software[a]

Pressure (GPa)	QS Site 1 (mm/s)	IS Site 1 (mm/s)	FWHM Site 1 (mm/s)	Δ Site 1	QS Site 2 (mm/s)	FWHM Site 2 (mm/s)	Δ Site 2	QS Site 3 (mm/s)	IS Site 3 (mm/s)	FWHM Site 3 (mm/s)	Δ Site 3	Reduced χ^2
3.2(3)	1.818(8)	0.955(1)	0.51	5.13	1.69(2)	0.63	0.58	0.80(3)	0.69(2)	0.63	0.41	1.36(6)
9.2(4)	2.07(3)	0.972(6)	0.46	3.88	1.66(2)	0.77	0.21	0.99(6)	0.68(1)	0.77	0.33	1.38(6)
13.1(2)	2.18(3)	0.975(6)	0.55	3.46	1.75(2)	0.82	0.11	0.93(5)	0.685(7)	0.82	0.21	1.20(5)
19.0(6)	2.46(3)	0.965(7)	0.41	4.57	1.99(1)	0.61	0.31	0.86(3)	0.690(8)	0.61	1.74	1.71(6)
25.3(1)	2.71(5)	0.940(7)	0.65	0.20	2.02(5)	0.71	1.30	0.744(7)	0.684(7)	1.40	1.41	2.15(7)
31.2(4)	2.99(2)	0.91(2)	0.65	0.20	2.10(1)	0.59	0.84	0.87(5)	0.71(3)	0.68	0.74	1.43(6)
36.5(2)	3.03(2)	0.98(2)	0.65	0.20	2.11(1)	0.65	0.77	0.65(6)	0.65(6)	0.84	0.60	1.45(6)
41.9(4)	3.14(1)	0.96(1)	0.65	0.20	2.17(1)	0.61	0.82	0.80(4)	0.69(2)	0.64	0.78	1.10(5)
48.0(6)	3.18(1)	0.95(2)	0.65	0.20	2.23(1)	0.62	0.81	0.89(5)	0.71(3)	0.72	0.70	1.32(6)
54.7(2)	3.157(9)	0.99(1)	0.65	0.20	2.334(8)	0.69	0.73	0.82(4)	0.72(3)	0.77	0.65	1.17(5)
60.9(9)	3.22(2)	0.98(2)	0.65	0.20	2.36(1)	0.67	0.75	0.92(5)	0.72 (3)	0.78	0.64	1.14(5)
65.8(8)	3.21(1)	0.96(1)	0.65	0.20	2.36(1)	0.69	0.75	0.88(4)	0.73(3)	0.73	0.66	1.18(5)
70.8(9)	3.24(1)	0.98(2)	0.65	0.20	2.35(1)	0.72	0.70	0.80(7)	0.72(5)	0.91	0.55	1.23(5)
76.7(9)	3.29(2)	0.94(2)	0.65	0.20	2.36(1)	0.66	0.76	0.96(7)	0.69(3)	0.80	0.62	1.36(6)
85(2)	3.31(1)	0.95(2)	0.65	0.20	2.38(1)	0.65	0.77	1.00(6)	0.69(3)	0.77	0.65	1.20(5)
94(3)	3.25(1)	0.91(2)	0.65	0.20	2.27(1)	0.68	0.74	1.04(9)	0.65(5)	1.00	0.50	1.69(6)
102(3)	3.256(6)	0.890(9)	0.49	0.51	2.337(6)	0.61	0.38	1.15(1)	0.662(9)	0.44	0.53	1.17(5)
111(3)	3.298(7)	0.863(5)	0.42	0.45	2.334(8)	0.54	0.51	1.15(2)	0.654(7)	0.41	0.67	1.47(6)
119(3)	3.310(8)	0.847(7)	0.47	0.51	2.369(8)	0.58	0.43	1.18(2)	0.627(8)	0.41	0.58	1.15(5)

[a]The relative weight of site 1, site 2, and site 3 were fixed to 34%, 47%, and 19%, respectively. These values were found with Monte Carlo searches combined with χ^2 and parameter correlation analysis as a function of pressure and cannot be fitted freely due to parameter correlations. The isomer shift for site 1 and site 2 are equivalent. Isomer shift values are with respect to α-iron metal. The physical thickness was fixed to 10 μm at all pressures ($\eta \approx 1.6$). The uncertainties are given in parentheses at the 68% confidence level for the last reported significant digit.

to 1.1 mm/s. In staurolite, the reported QS and IS values for fourfold iron are 1.3 to 1.6 mm/s and ~1 mm/s, respectively [*Dowty*, 1972], whereas in chromite, the fourfold ferrous iron has QS values ranging from 0.5 to 1.6 mm/s and IS values of 0.9 to 1.1 mm/s [*Chen et al.*, 1992; *Kuno et al.*, 2000]. Fourfold ferric iron has slightly higher QS values and significantly lower IS values than fourfold ferrous iron. For example, melilite has two distinct tetrahedral ferric sites with QS values ranging from 1 to 1.9 mm/s and IS values of 0.1 to 0.3 mm/s [*Hamada and Akasaka*, 2013].

Fivefold ferrous iron has a larger spread of hyperfine parameters as reported in literature, with QS and IS values ranging from 0.4 to 2.7 mm/s and from about 0.2 to 1.1 mm/s, respectively, depending on the crystal structure and interpretation of hyperfine parameters [*Burns*, 1994]. Grandidierite and kornerupine each have a fivefold ferrous site with QS and IS values of ~1.7 mm/s and ~1.1 mm/s, respectively [*Seifert and Olesch*, 1977; *Zhe et al.*, 2000]. Also, in vesuvianite a site with QS and IS values of 0.6 mm/s and 0.33 to 0.37 mm/s was attributed to fivefold ferrous iron [*Malczewski et al.*, 2006]. For natural hibonite, *Burns and Burns* [1984] attribute a site with QS and IS values of 2.2 mm/s and 0.3 mm/s, respectively, to fivefold ferric iron and a site with QS and IS values of 2.2 mm/s and 1 mm/s, respectively, to fivefold ferrous iron. Unlike grandidierite and kornerupine, where the fivefold and sixfold sites are distinct, the three to five sites in the spectra for vesuvianite and hibonite have significant overlap, and alternative models may possibly fit the spectra as well. Thus, it is unclear if QS values of 0.4 to 2.7 mm/s establish a plausible strict range for fivefold ferrous iron in crystalline

Table 4. Error Correlation Matrix for the Fitted Hyperfine Parameters for Rhyolitic Glass at 60.9 GPa, Acquired With CONUSS[a]

	QS Site 1	QS Site 2	QS Site 3	IS Site 1	IS Site 3
QS site 1	1.000	−0.212	0.314	−0.483	−0.448
QS site 2	−0.212	1.000	0.487	−0.044	0.385
QS site 3	0.314	0.487	1.000	−0.235	0.407
IS site 1	−0.483	−0.044	−0.235	1.000	0.608
IS site 3	−0.448	0.385	0.407	0.608	1.000

[a]Perfect correlation corresponds to ±1 and a lack of correlation corresponds to 0. Thickness, thickness distribution, QS distribution, attachment parameter, and weight fractions of the different sites were fixed.

Table 5. Best Fit Hyperfine Parameters for Basaltic Glass and the Corresponding Reduced χ^2 From Fitting the Time Domain Synchrotron Mössbauer Spectra With the CONUSS Software[a]

Pressure (GPa)	QS Site 1 (mm/s)	IS Site 1 (mm/s)	FWHM Site 1 (mm/s)	Δ Site 1	QS Site 2 (mm/s)	FWHM Site 2 (mm/s)	Δ Site 2	QS Site 3 (mm/s)	IS Site 3 (mm/s)	FWHM Site 3 (mm/s)	Δ Site 3	η	Reduced χ^2
1.8(3)	2.003(3)	1.015(4)	0.57	0.22	1.63(2)	1.02	0.53	1.08(4)	0.704(4)	0.75	0.46	6.87	1.48(6)
5(1)	1.994(5)	1.021(3)	0.59	0.23	1.60(1)	0.94	0.31	1.10(3)	0.664(3)	0.66	0.29	8.07	2.89(8)
6.5(4)	2.047(3)	1.007(4)	0.57	0.27	1.64(3)	0.69	0.45	1.02(6)	0.630(4)	0.90	0.70	8.08	1.56(6)
8.2(5)	2.065(3)	1.019(4)	0.59	0.19	1.62(2)	0.71	0.34	1.09(3)	0.681(4)	0.72	0.95	7.87	1.31(5)
12.6(7)	2.328(2)	1.030(4)	0.61	0.13	1.679(7)	0.52	0.41	1.25(6)	0.688(4)	0.75	1.30	8.92	1.30(6)
18.8(2)	2.481(2)	1.029(4)	0.60	0.22	1.743(7)	0.51	0.42	1.40(7)	0.675(4)	0.84	1.17	9.22	1.40(6)
25.4(1)	2.576(2)	1.006(5)	0.64	0.28	1.79(1)	0.57	0.39	1.53(8)	0.685(5)	0.93	1.09	9.19	1.26(5)
33.7(1)	2.650(2)	0.983(5)	0.62	0.23	1.745(9)	0.52	0.11	1.42(1)	0.628(5)	0.51	0.75	8.99	1.49(6)
38.9(1)	2.704(2)	0.960(5)	0.64	0.24	1.72(1)	0.55	0.14	1.40(2)	0.591(5)	0.49	1.00	8.87	1.21(5)
45.4(1)	2.724(2)	0.939(5)	0.64	0.19	1.680(9)	0.52	0.14	1.41(1)	0.591(5)	0.39	0.86	9.25	1.62(6)
52.9(3)	2.831(2)	0.959(4)	0.67	0.23	1.764(8)	0.52	0.29	1.48(1)	0.520(4)	0.40	1.07	9.28	1.16(5)
60.5(6)	2.869(2)	0.938(4)	0.68	0.27	1.772(7)	0.52	0.45	1.47(1)	0.493(4)	0.38	1.14	9.28	1.09(5)
74.9(7)	2.925(2)	0.934(4)	0.68	0.30	1.811(6)	0.52	0.49	1.45(1)	0.445(4)	0.36	1.00	7.91	1.39(6)
84(2)	2.919(2)	0.932(4)	0.68	0.30	1.798(6)	0.52	0.53	1.43(1)	0.426(4)	0.35	0.98	7.63	1.56(6)
89.0(6)	2.938(3)	0.912(4)	0.69	0.30	1.772(7)	0.56	0.58	1.40(1)	0.404(5)	0.34	0.86	7.45	1.90(7)
96.9(9)	2.938(2)	0.895(4)	0.71	0.38	1.756(6)	0.63	0.70	1.338(9)	0.378(4)	0.31	0.80	7.21	1.63(6)

[a]The relative weight of site 1, site 2, and site 3 were fixed to 62%, 26%, and 12%, respectively, between 1.8 and 84 GPa. At 89.0 and 96.9 GPa, the relative weights are 60%, 26%, and 14%, respectively. The isomer shift for site 1 and site 2 are equivalent. Isomer shift values are with respect to α-iron metal. The uncertainties are given in parentheses at the 68% confidence level for the last reported significant digit.

phases, because different types of fivefold iron geometries result in a wide variability of quadrupole splitting values. Optical spectra of grandidierite and joaquinite support the idea that fivefold iron geometries can be very dissimilar from each other [*Rossman and Taran*, 2001].

At ambient pressure, the majority site in rhyolitic and basaltic glasses shows hyperfine parameters typical for sixfold and possibly fivefold ferrous iron in silicate minerals. The minority site has a QS value that falls between those associated to fourfold ferrous and ferric iron in minerals and may represent a less distorted fivefold site. The presence of predominantly fivefold and distorted sixfold ferrous iron are consistent with the absorption spectra (see section 3 for more details). The IS value for the minority site in both glasses is about 0.7 mm/s, which is higher than that reported for Fe^{3+} in minerals [*Mysen*, 1987; *Burns*, 1994; *Dyar et al*., 2006]. The silicate glasses were synthesized under reducing conditions (see section 2.2). The rhyolitic glass remained optically colorless at all pressures and is therefore unlikely that the minority site with a weight fraction of 20% is Fe^{3+}. Using the extended Voigt-based fitting method [*Alberto et al*., 1996], *Rossano et al*. [1999] did not detect ferric iron in the tektites in their study although the $Fe^{3+}/\Sigma Fe_{tot}$ ranges from 5 to 9%, as determined from coulometric titration. The minority site in the tektites has QS and IS values of ~1 mm/s and ~0.6 mm/s, respectively, and is attributed to tetrahedral Fe^{2+} [*Rossano et al*., 1999], consistent with the minority site in the rhyolitic and basaltic glasses in this study at room pressure-temperature conditions. One cannot rule out that the lower isomer shift value is a result of electron exchange between ferrous iron and small amounts of ferric iron in the glasses [*Burns*, 1991; *Burns*, 1994; *Dyar et al*., 2006], but based upon the optical absorption spectra showing no detectable ferric iron features, the amount of ferric iron would indeed be very small.

Table 6. Error Correlation Matrix for the Fitted Hyperfine Parameters for Basaltic Glass at 60.5 GPa, Acquired With CONUSS[a]

	QS Site 1	QS Site 2	QS Site 3	IS Site 1	IS Site 3
QS site 1	1.000	0.553	0.393	0.195	0.413
QS site 2	0.553	1.000	0.724	0.165	0.480
QS site 3	0.393	0.724	1.000	−0.106	0.296
IS site 1	0.195	0.165	−0.106	1.000	0.746
IS site 3	0.413	0.480	0.296	0.746	1.000

[a]Thickness, thickness distribution, the QS distribution, attachment parameter, and weight fractions of the different sites were fixed.

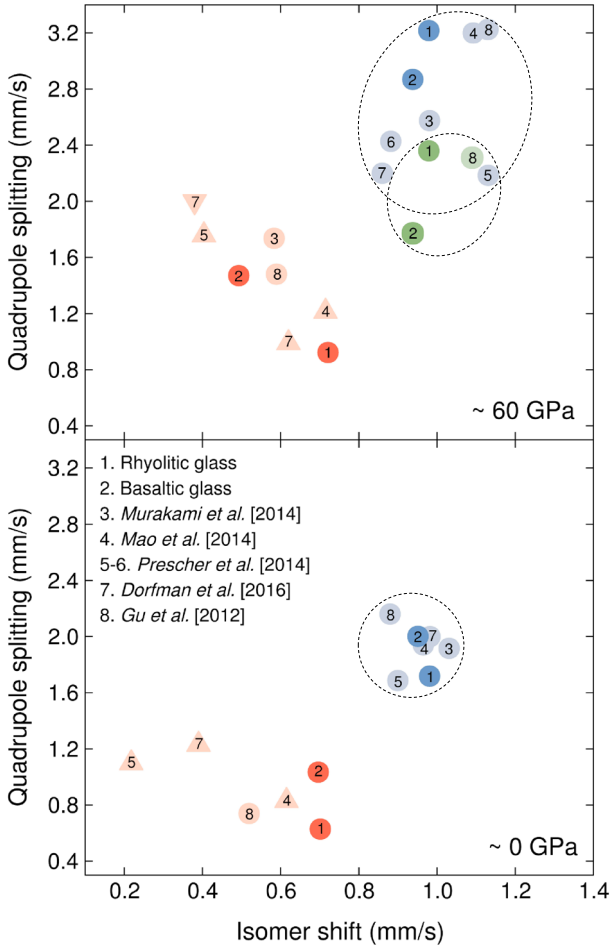

Figure 7. Quadrupole splitting versus isomer shift at about (bottom) 0 GPa and (top) 60 GPa for high-pressure synchrotron Mössbauer studies on silicate glasses. Our study is in bold colors, whereas previous studies are in pastel colors. See Table 1 for compositions of the glasses. Blue, green, and red circles represent Fe^{2+} sites with relatively high, intermediate, and low quadrupole splitting values, respectively. Triangles have been interpreted as Fe^{3+} sites; the inverted triangle denotes low-spin Fe^{3+} [*Dorfman et al.*, 2016]. All isomer shifts are with respect to α-iron, except for the Al-bearing silicate glass from *Gu et al.* [2012], which is with respect to a stainless steel foil. For the Al-free silicate glass, *Gu et al.* [2012] do not report isomer shifts. *Murakami et al.* [2014], *Mao et al.* [2014], and *Prescher et al.* [2014] fit their spectra with two sites, a high QS site and a low QS site; thus, there is no intermediate QS site for those studies. Figure 7 (bottom) is at 1 bar for all studies, except for *Prescher et al.* [2014] where their lowest pressure is at 0.18 GPa for the Fe^{3+}-bearing glass in a Ne pressure medium (label #5 here). There was no low-pressure measurement for the Fe^{3+}-free glass from *Prescher et al.* [2014]. The high-pressure measurements for rhyolitic and basaltic glass were measured at 60.9 and 60.5 GPa, respectively. The high-pressure measurements for *Murakami et al.* [2014], *Mao et al.* [2014], *Prescher et al.* [2014] with Fe^{3+}, *Prescher et al.* [2014] without Fe^{3+}, *Dorfman et al.* [2016], and *Gu et al.* [2012] were conducted at 58, 55, 56, 61, 57, and 58 GPa, respectively.

4.2. Coordination Environments at High Pressure

At high pressure, the increase of the QS values of site 1 with pressure up to about 30 GPa is likely associated with glass densification that results in an increase in the coordination number of that site from around four to eight, and perhaps higher than eight. *Bajgain et al.* [2015] presented density functional theory-based results on the behavior of hydrous and anhydrous basaltic melts with pressure, noting steep gradients in the coordination increases of Ca-O, Na-O, and Si-O from ambient pressure to about 40 GPa. This particular densification does not appear to affect the electron density near the nucleus of iron, as evidenced by the relatively flat trend of the IS up to about 20 GPa for both glasses. The QS and IS values of site 2 in rhyolitic and basaltic glass are consistent with fivefold and sixfold ferrous iron in minerals. At elevated pressure, a third site is required to fit the glass spectra. Site 3 in the rhyolitic glass has a QS value that increases from about 0.7 to 1.2 mm/s and an IS value that plateaus at about 0.7 mm/s up to 80 GPa, likely remaining in a low-coordinated site environment to high pressure.

In the basaltic glass, the IS values start to decrease from 0.7 mm/s to 0.5 mm/s at about 25 GPa with a very similar trend compared to that reported by *Murakami et al.* [2014]. *Murakami et al.* [2014] propose that the decrease in IS values is due to a change in the spin state from high spin to intermediate spin. For Al-bearing enstatite glass, *Gu et al.* [2012] observe comparable IS values (0.5–0.7 mm/s relative to a stainless steel reference absorber) for the site with low QS values and attribute it to low-spin ferrous iron. We do not attribute site 3 to intermediate-spin or low-spin iron because of its existence even at low pressures with significant weight fractions, 19% for the rhyolitic glass and 12% for the basaltic glass without significant change at higher pressures. We attribute the decreasing trend of the isomer shift values to glass densification and near-neighbor coordination increases that start to have a stronger effect on the electron density near the nucleus.

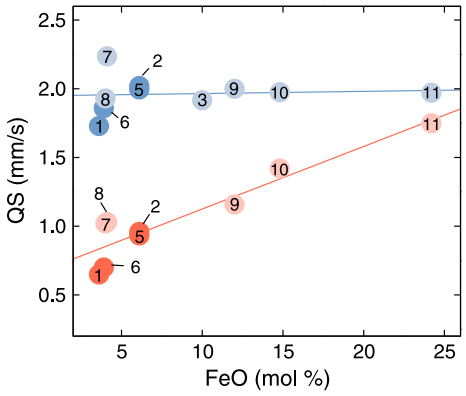

Figure 8. Quadrupole splitting as a function of FeO concentration at ~0 GPa for a range of glasses. Rhyolitic glass (this study) (1), basaltic glass (this study) (2), *Murakami et al.* [2014] (3), andesitic glass (this study) (5), dacitic glass (this study) (6), *Alberto et al.* [1996] (7), *Rossano et al.* [1999] (8), and *Jackson et al.* [2005] (9–11). See Table 1 for compositions of the silicate glasses. *Jackson et al.* [2005] do not report the hyperfine parameters for the individual sites. Thus, the quadrupole splitting values are estimated from their fits. The total concentration of FeO in a glass affects the quadrupole splitting of the minority (lower QS) site more than the concentration of other cations above a certain threshold of FeO, likely due to iron-iron interactions. For this reason, the results of *Jackson et al.* [2005] are not included in Figure 9.

4.3. Comparison With Previous Studies

A comparison of our results to previous room temperature studies is shown in Figure 7, where we plot QS against IS values for a variety of reduced and oxidized silicate glasses for pressures up to ~60 GPa. At ambient pressure, the hyperfine parameters for the dominant ferrous iron site are tightly constrained with QS and IS values ranging from 1.7 to 2 mm/s and from 0.9 to 1 mm/s, respectively. The QS values for all sites generally increase with pressure. At higher pressures, the increased scatter of hyperfine parameters is likely a result of compositional effects that become more prominent. At high pressure, the hyperfine parameters of the ferrous site with a low QS value are similar to those reported for ferric iron. Therefore, if there is a lack of constraint on the behavior of this site from low-pressure data and/or complementary spectroscopic data, it can be difficult to interpret. The weights of such sites obtained from Mössbauer studies can also conceivably trade for each other making quantitative assignments uncertain. In our study of the rhyolitic glass, this site has a weight fraction of about 20%, which clearly exceeds the possible Fe^{3+} content.

4.4. Trends With Composition

QS values are affected by the coordination environment, which may be influenced by the type and number of cations in the vicinity of the iron atoms. Here we examine the effect of different cations on the QS values of ferrous iron in combination with the effect of the molar quantity of Na_2O, K_2O, MgO, CaO, SiO_2, and Al_2O_3 with respect to FeO. Studies on glasses that reported a detectable amount of ferric iron ($Fe^{3+}/\Sigma Fe_{tot} > 6\%$) were not included in this analysis due to the strong effect of ferric iron on the local coordination environment of ferrous sites [*Alberto et al.*, 1996; *Wilke et al.*, 2005]. Asymmetric peak shapes, characteristic of silicate glasses, require correlated distributions to fit the spectra and cannot be quantitatively compared to studies that do not use correlated distributions [*Rossano et al.*, 1999]. Thus, we do not include the results of those studies [e.g., *Aramu et al.*, 1994; *Costa et al.*, 2014; *Gu et al.*, 2012]. Although *Dunlap et al.* [1998] use correlated distributions, they do not report the compositions of the natural tektites in their study; thus, their results are not included in our compositional analysis. At high pressures, *Gu et al.* [2012] fit their data using FWHM values ranging from 1 to 2 mm/s, which is larger than has been used in previous studies on silicate glasses, in particular those studies using a radioactive source, and is likely a result of not implementing correlated distributions.

Large concentrations of FeO (above about 10 mol %) appear to result in iron-iron interactions that affect the quadrupole splitting of the minority (lower QS) site more than the other oxides that were considered in our compositional analysis (Figure 8). There is a positive trend in the quadrupole splitting of the minority site with increasing FeO concentration, such that the effect of compositional differences on the minority site can only be resolved at low FeO concentrations. For this reason, we do not include the iron-rich silicate glasses of *Jackson et al.*, [2005] in our detailed compositional analysis. By including only reduced glasses with low FeO concentrations and comparing studies that use similar methods to fit their data, it becomes possible to examine the effect of composition on the QS of ferrous iron in a self-consistent manner.

At ambient pressure, we observe a negative correlation between QS values and Na_2O/FeO, K_2O/FeO and $(Na_2O + K_2O)/FeO$, and a positive correlation between QS values and CaO/FeO and (MgO + CaO)/FeO for

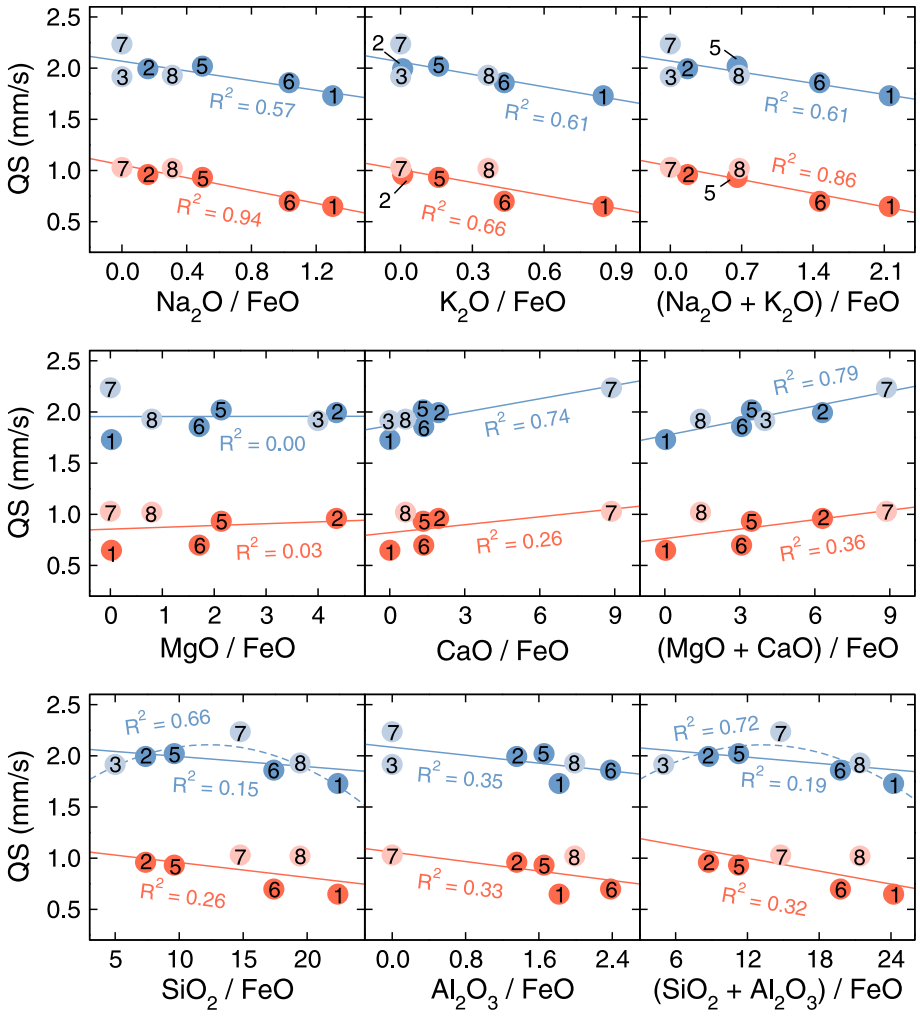

Figure 9. Quadrupole splitting as a function of the oxide mole ratios, Na_2O/FeO, K_2O/FeO, (Na_2O + K_2O)/FeO, MgO/FeO, CaO/FeO, (MgO + CaO)/FeO, SiO_2/FeO, Al_2O_3/FeO, and (SiO_2 + Al_2O_3)/FeO at ~0 GPa. Only reduced glasses ($Fe^{3+}/\Sigma Fe_{tot}$ below 6%) are included in this figure due to the strong effect of ferric iron on the coordination environment of ferrous sites [*Alberto et al.*, 1996; *Wilke et al.*, 2005; *Jackson et al.*, 2005]. Rhyolitic glass (this study) (1), basaltic glass (this study) (2), *Murakami et al.* [2014] (3), *Prescher et al.* [2014] (4), andesitic glass (this study) (5), dacitic glass (this study) (6), *Alberto et al.* [1996] (7), and *Rossano et al.* [1999] (8). Fitting quadratic trends to the majority sites in the plots of QS versus SiO_2/FeO and QS versus (SiO_2 + Al_2O_3)/FeO leads to better R^2 values.

both the majority and minority sites (Figure 9). The Mg-free Ca-silicate glass of *Alberto et al.* [1996] has relatively large QS values for the majority site, which is likely affected by CaO. The result is a very weak correlation for MgO/FeO versus QS and a strong correlation for (MgO + CaO)/FeO versus QS for the majority site. Ferrous iron in mafic melts, containing more MgO and CaO, is likely to be more distorted and/or have a higher coordination than ferrous iron in felsic melts, containing more Na_2O and K_2O. The effect of SiO_2 and Al_2O_3 is weaker. One can interpret the effect of SiO_2 with respect to FeO as having a weak negative correlation or a moderately strong quadratic relationship. With the amount of data available at present, it appears that the type of network-modifying cations in the glass have a stronger effect on the quadrupole splitting (and likely coordination environment) of iron than the silica or alumina content. As discussed earlier, IS values have also been used as an indicator for coordination [*Mysen*, 1987; *Dyar et al.*, 2006]. However, when plotted against compositional ratios or against absolute oxide content, the IS values are scattered with low R^2 values (typically 0 to 0.2) (Figure S1 in the supporting information). It appears that IS values are not sensitive to composition in silicate glasses. In fact, an enstatite glass with the composition $(Mg_{0.8}Fe_{0.2})SiO_3$ [*Murakami et al.*, 2014] shows very similar IS values, but different QS values than the compositionally-complex basaltic glass in this study (Figures 6 and 7).

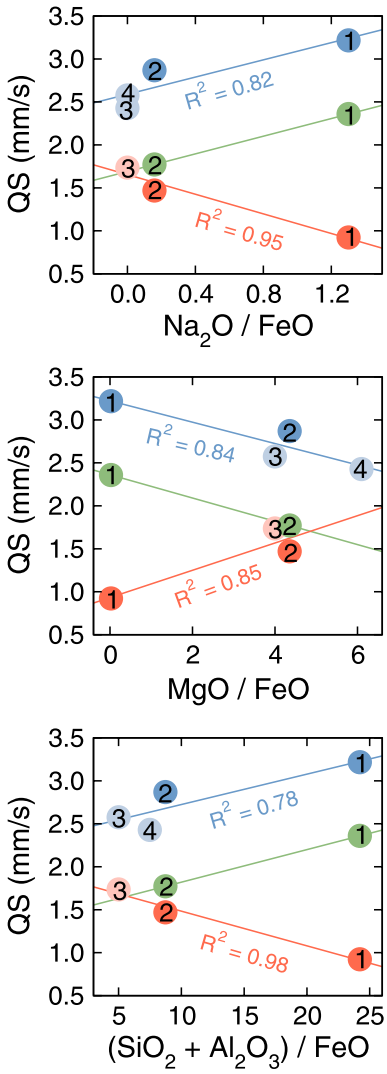

Figure 10. Quadrupole splitting as a function of the oxide mole ratios, Na_2O/FeO, MgO/FeO, and (SiO_2 + Al_2O_3)/FeO at ~60 GPa. The high-pressure measurements for rhyolitic glass (1) and basaltic glass (2) were conducted at 60.9 and 60.5 GPa, respectively, and the high-pressure measurements for *Murakami et al.* [2014] (3) and *Prescher et al.* [2014] (4) were conducted at 58 and 61 GPa, respectively. See text for discussion.

At high pressure, only three studies on reduced glasses use correlated hyperfine parameter distributions to fit the spectra [*Murakami et al.*, 2014; *Prescher et al.*, 2014; this study]. We restrict the figures to ones with the most spread in compositional space: Na_2O/FeO, MgO/FeO, and (SiO_2 + Al_2O_3)/FeO. At ~60 GPa, the trend for the majority site is reversed, such that QS values are now positively correlated with Na_2O/FeO and negatively correlated with MgO/FeO (Figure 10). The rhyolitic glass has a much larger distribution of site environments compared to the other glasses, indicating that felsic melts may be expected to have a larger distribution of ferrous iron sites than mafic melts at high pressures.

5. Conclusions

Our results indicate that ferrous iron in rhyolitic and basaltic glass experiences an increase in coordination with increasing pressure. The increase in coordination is likely accompanied by variable distortions in the environments. A decreasing trend of the isomer shift values at high pressures can be associated with glass densification and steep gradients of coordination changes in the different glasses, noting that this trend occurs at lower pressures in basaltic glass compared to rhyolitic glass. Over the pressure range studied, these local environmental changes occur without the iron atoms undergoing high-spin to low-spin transitions but would nevertheless affect physical and transport properties. The volume of iron's coordination environment is a critical factor determining iron's spin transition pressure. It has been shown that the average coordination of iron in silicate melts and glasses of the same composition and oxidation state are similar when the glasses are produced with a fast quench rate [*Wilke et al.*, 2005]. As such, the characteristics of the spin transition in silicate melts may be similar to that of glasses, although will likely occur over an even broader pressure range due to thermal effects on the spin populations and structural disorder in the melt. With the assumption that silicate glasses can be used to model some of the behavior in silicate melts, our study predicts that ferrous iron in chemically complex silicate-rich melts in the lower mantle likely exists in a high-spin state.

We compare the results of studies that used similar methods in fitting their Mössbauer spectra of reduced glasses and observe a negative relationship between quadrupole splitting and the concentration of Na_2O and K_2O with respect to FeO at ambient pressure. At high pressure, this relationship turns into a positive trend of quadrupole splitting for the majority site and a negative trend for the minority site. Our results indicate that at high pressure, felsic melts may have a larger distribution in ferrous iron site geometries while

mafic melts have ferrous iron site geometries that are more similar to each other. To the extent that the distribution of available coordination environments affects element partitioning between the solid and the melt, more silica-poor melts would accommodate a smaller variety of cations compared to more silica-rich melts at lower mantle pressures.

Acknowledgments
We would like to thank E.E. Alp and W. Bi for isomer shift measurements of the reference stainless steel foils, D. Zhang and R.A. Morrison for their assistance with the measurements, and T.S. Toellner for valuable discussions. We are thankful to NSF-CSEDI-EAR-1600956, NSF-EAR-1322082, and the Keck Institute for Space Studies for financial support. We acknowledge COMPRES for partial support of Sector 3 and the Mössbauer Laboratory at the Advanced Photon Source (APS). This work was supported by the French ANR Program (2011JS56 004 01, FrIHIDDA) and by the Region Nord-Pas de Calais to M.R. Ruby fluorescence measurements were conducted at GSECARS and HPCAT at the APS. Use of the APS is supported by U.S. DOE, Office of Science (DE-AC02-06CH11357). We thank two anonymous reviewers for their thoughtful comments. The composition of the glasses, the hyperfine data, and select correlation matrices are tabulated in this manuscript; additional data may be obtained from N.V. Solomatova. The CONUSS software, developed by W. Sturhahn, is open source and available at http://www.nrixs.com/conuss.html.

References

Akahama, Y., and H. Kawamura (2006), Pressure calibration of diamond anvil Raman gauge to 310 GPa, *J. Appl. Phys.*, *100*, 043516, doi:10.1063/1.2335683.

Alberto, H. V., J. P. da Cunha, B. O. Mysen, J. M. Gil, and N. A. de Campos (1996), Analysis of Mössbauer spectra of silicate glasses using a two-dimensional Gaussian distribution of hyperfine parameters, *J. Non-Cryst. Solids*, *194*(1–2), 48–57, doi:10.1016/0022-3093(95)00463-7.

Aramu, F., P. Brovetto, V. Maxia, M. Salis, and G. Spano (1994), Mössbauer spectroscopy of tektites, *Il Nuovo Cimento D*, *16*(6), 621–626, doi:10.1007/BF02451660.

Bajgain, S., D. B. Ghosh, and B. B. Karki (2015), Structure and density of basaltic melts at mantle conditions from first-principles simulations, *Nat. Commun.*, *6*, doi:10.1038/ncomms9578.

Behrens, H., and A. Stuke (2003), Quantification of H_2O contents in silicate glasses using IR spectroscopy: A calibration based on hydrous glasses analyzed by Karl-Fischer titration, *Glass Sci. Technol.*, *76*(4), 176–189.

Boon, J. A., and W. S. Fyfe (1972), The coordination number of ferrous ions in silicate glasses, *Chem. Geol.*, *10*(4), 287–298, doi:10.1016/0009-2541(72)90023-X.

Burns, R. G., and V. M. Burns (1984), Optical and Mössbauer spectra of transition-metal-doped corundum and periclase, *Adv. Ceram.*, *10*, 46.

Burns, R. G. (1985), Thermodynamic data from crystal field spectra, *Rev. Mineral. Geochem.*, *14*(1), 277–316.

Burns, R. G. (1991), Mixed valency minerals: Influences of crystal structures on optical and Mössbauer spectra, in *Mixed Valency Systems: Applications in Chemistry, Physics and Biology*, pp. 175–199, Springer, Netherlands.

Burns, R. G. (1993), Mineralogical applications of crystal field theory vol. 5, pp. 314–319, Cambridge Univ. Press.

Burns, R. G. (1994), Mineral Mössbauer spectroscopy: Correlations between chemical shift and quadrupole splitting parameters, *Hyperfine Interact.*, *91*(1), 739–745, doi:10.1007/BF02064600.

Carl, R., S. Gerlach, and C. Rüssel (2007), The effect of composition on UV–Vis–NIR spectra of iron doped glasses in the systems $Na_2O/MgO/SiO_2$ and $Na_2O/MgO/Al_2O_3/SiO_2$, *J. Non-Cryst. Solids*, *353*(3), 244–249, doi:10.1016/j.jnoncrysol.2006.11.010.

Chen, Y. L., B. F. Xu, J. G. Chen, and Y. Y. Ge (1992), Fe^{2+}–Fe^{3+} ordered distribution in chromite spinels, *Phys. Chem. Miner.*, *19*(4), 255–259, doi:10.1007/BF00202316.

Costa, T. M. H., M. R. Gallas, E. V. Benvenutti, and J. A. H. Da Jornada (1997), Infrared and thermogravimetric study of high pressure consolidation in alkoxide silica gel powders, *J. Non-Cryst. Solids*, *220*(2–3), 195–201.

Costa, B. F. O., G. Klingelhöfer, and E. I. Alves (2014), ^{57}Fe Mössbauer spectroscopy studies of Tektites from Khon Kaen, Ne Thailand, *Hyperfine Interact.*, *224*(1–3), 51, doi:10.1007/s10751-013-0769-x.

Cottrell, E., and K. A. Kelley (2011), The oxidation state of Fe in MORB glasses and the oxygen fugacity of the upper mantle, *Earth Planet. Sci. Lett.*, *305*(3–4), 270–282, doi:10.1016/j.epsl.2011.03.014.

Dauphas, N., et al. (2014), Magma redox and structural controls on iron isotope variations in Earth's mantle and crust, *Earth Planet. Sci. Lett.*, *398*, 127–140, doi:10.1016/j.epsl.2014.04.033.

Dewaele, A., M. Torrent, P. Loubeyre, and M. Mezouar (2008), Compression curves of transition metals in the Mbar range: Experiments and projector augmented-wave calculations, *Phys. Rev. B*, *78*(10), 104102, doi:10.1103/PhysRevB.78.104102.

Dorfman, S. M., et al. (2016), Electronic transitions of iron in almandine-composition glass to 91 GPa, *Am. Mineral.*, *101*(7), 1659–1667.

Dowty, E. (1972), Site distribution of iron in staurolite, *Earth Planet. Sci. Lett.*, *15*, 72–74, doi:10.1016/0012-821X(72)90031-3.

Dunlap, R. A., D. A. Eelman, and G. R. MacKay (1998), A Mössbauer effect investigation of correlated hyperfine parameters in natural glasses (tektites), *J. Non-Cryst. Solids*, *223*(1–2), 141–146, doi:10.1016/S0022-3093(97)00364-5.

Dyar, M. D., D. G. Agresti, M. W. Schaefer, C. A. Grant, and E. C. Sklute (2006), Mössbauer spectroscopy of Earth and planetary materials, *Annu. Rev. Earth Planet. Sci.*, *34*, 83–125, doi:10.1146/annurev.earth.34.031405.125049.

ElBatal, F. H., M. S. Selim, S. Y. Marzouk, and M. A. Azooz (2007), UV-vis absorption of the transition metal-doped SiO_2–B_2O_3–Na_2O glasses, *Physica B*, *398*(1), 126–134, doi:10.1016/j.physb.2007.05.004.

Farges, F., S. Rossano, Y. Lefrere, M. Wilke, and G. E. Brown Jr. (2005), Iron in silicate glasses: A systematic analysis of pre-edge, XANES and EXAFS features, *Phys. Scr.*, *2005*(T115), 957, doi:10.1238/Physica.Topical.115a00957.

Goldman, D. S., and G. R. Rossman (1977), The spectra of iron in orthopyroxene revisited: The splitting of the ground state, *Am. Mineral.*, *62*, 151–157.

Gu, C., K. Catalli, B. Grocholski, L. Gao, E. Alp, P. Chow, Y. Xiao, H. Cynn, W. J. Evans, and S. H. Shim (2012), Electronic structure of iron in magnesium silicate glasses at high pressure, *Geophys. Res. Lett.*, *39*, L24304, doi:10.1029/2012GL053950.

Guo, X., R. A. Lange, and Y. Ai (2013), The density and compressibility of CaO–FeO–SiO_2 liquids at one bar: Evidence for four-coordinated Fe^{2+} in the $CaFeO_2$ component, *Geochim. Cosmochim. Acta*, *120*, 206–219, doi:10.1016/j.gca.2013.06.007.

Hamada, M., and M. Akasaka (2013), Distribution of cations at two tetrahedral sites in $Ca_2MgSi_2O_7$-$Ca_2Fe^{3+}AlSiO_7$ series synthetic melilite and its relation to incommensurate structure, *Phys. Chem. Miner.*, *40*, 259–270, doi:10.1007/s00269-013-0566-8.

Iwamoto, N., Y. Tsunawaki, H. Nakagawa, T. Yoshimura, and N. Wakabayashi (1978), Investigation of calcium-iron-silicate glasses by the Mössbauer method, *J. Non-Cryst. Solids*, *29*(3), 347–356, doi:10.1016/0022-3093(78)90155-2.

Jackson, W. E., F. Farges, M. Yeager, P. A. Mabrouk, S. Rossano, G. A. Waychunas, E. Solomon, and G. E. Brown (2005), Multi-spectroscopic study of Fe (II) in silicate glasses: Implications for the coordination environment of Fe (II) in silicate melts, *Geochim. Cosmochim. Acta*, *69*(17), 4315–4332, doi:10.1016/j.gca.2005.01.008.

Karakassides, M. A., D. Gournis, and D. Petridis (1999), An infrared reflectance study of Si–O vibrations in thermally treated alkali-saturated montmorillonites, *Clay Miner.*, *34*(3), 429–429, doi:10.1180/000985599546334.

Kido, L., M. Müller, and C. Rüssel (2006), Redox reactions during temperature change in soda-lime–silicate melts doped with copper and iron or copper and manganese, *J. Non-Cryst. Solids*, *352*(38–39), 4062–4068, doi:10.1016/j.jnoncrysol.2006.06.027.

Klement, R., J. Kraxner, and M. Liška (2009), Spectroscopic analysis of iron doped glasses with composition close to the E-glass: A preliminary study, *Ceram. Silik.*, *53*, 180–183.

Kuno, A., R. Santos, M. Matsuo, and B. Takano (2000), Characterization of natural chromite samples from ophiolite complexes in the Philippines by ^{57}Fe Mössbauer spectroscopy, *J. Radioanal. Nucl. Chem.*, *246*, 79–83, doi:10.1023/A:1006724913427.

Madejová, J., and P. Komadel (2001), Baseline studies of the clay minerals society source clays: Infrared methods, *Clays Clay Miner.*, *49*(5), 410–432.

Malczewski, D., J. E. Frąckowiak, and E. V. Galuskin (2006), ^{57}Fe Mössbauer spectroscopy and x-ray diffraction study of some complex metamict minerals, in *ICAME 2005*, pp. 529–536, Springer, Berlin, Heidelberg.

Manghnani, M. H., J. R. Ferraro, and L. J. Basile (1974), A study of Na_2O-TiO_2-SiO_2 glasses by infrared spectroscopy, *Appl. Spectrosc.*, *28*(3), 256–259, doi:10.1366/000370274774332542.

Mao, H. K., J. Xu, and P. M. Bell (1986), Calibration of the ruby pressure gauge to 800 kbar under quasi-hydrostatic conditions, *J. Geophys. Res.*, *91*, 4673–4676, doi:10.1029/JB091iB05p04673.

Mao, Z., J. F. Lin, J. Yang, J. Wu, H. C. Watson, Y. Xiao, P. Chow, and J. Zhao (2014), Spin and valence states of iron in Al-bearing silicate glass at high pressures studied by synchrotron Mössbauer and X-ray emission spectroscopy, *Am. Mineral.*, *99*(2–3), 415–423, doi:10.2138/am.2014.4490.

Maruyama, S., M. Santosh, and D. Zhao (2007), Superplume, supercontinent, and post-perovskite: Mantle dynamics and anti-plate tectonics on the core–mantle boundary, *Gondwana Res.*, *11*(1–2), 7–37, doi:10.1016/j.gr.2006.06.003.

Mössbauer, R. L. (1962), Recoilless nuclear resonance absorption, *Annu. Rev. Nucl. Sci.*, *12*(1), 123–152, doi:10.1146/annurev.ns.12.120162.001011.

Murakami, M., A. F. Goncharov, N. Hirao, R. Masuda, T. Mitsui, S. M. Thomas, and C. R. Bina (2014), High-pressure radiative conductivity of dense silicate glasses with potential implications for dark magmas, *Nat. Commun.*, *5*, 5428.

Mysen, B. O. (1987), Redox equilibria and coordination of Fe^{2+} and Fe^{3+} in silicate glasses from ^{57}Fe Mössbauer spectroscopy, *J. Non-Cryst. Solids*, *95–96*, 247–254, doi:10.1016/S0022-3093(87)80117-5.

Newman, S., E. M. Stolper, and S. Epstein (1986), Measurement of water in rhyolitic glasses: Calibration of an infrared spectroscopic technique, *Am. Mineral.*, *71*(11–12), 1527–1541.

Nolet, D. A. (1980), Optical absorption and Mössbauer spectra of Fe, Ti silicate glasses, *J. Non-Cryst. Solids*, *37*(1), 99–110, doi:10.1016/0022-3093(80)90482-2.

Nomura, R., H. Ozawa, S. Tateno, K. Hirose, J. Hernlund, S. Muto, H. Ishii, and N. Hiraoka (2011), Spin crossover and iron-rich silicate melt in the Earth's deep mantle, *Nature*, *473*(7346), 199–202, doi:10.1038/nature09940.

Pandya, N., D. W. Muenow, and S. K. Sharma (1992), The effect of bulk composition on the speciation of water in submarine volcanic glasses, *Geochim. Cosmochim. Acta*, *56*(5), 1875–1883, doi:10.1016/0016-7037(92)90317-C.

Prescher, C., C. Weigel, C. McCammon, O. Narygina, V. Potapkin, I. Kupenko, R. Sinmyo, A. I. Chumakov, and L. Dubrovinsky (2014), Iron spin state in silicate glass at high pressure: Implications for melts in the Earth's lower mantle, *Earth Planet. Sci. Lett.*, *385*, 130–136, doi:10.1016/j.epsl.2013.10.040.

Ramo, D. M., and L. Stixrude (2014), Spin crossover in Fe_2SiO_4 liquid at high pressure, *Geophys. Res. Lett.*, *41*, 4512–4518, doi:10.1002/2014GL060473.

Rossano, S., E. Balan, G. Morin, J. P. Bauer, G. Calas, and C. Brouder (1999), ^{57}Fe Mössbauer spectroscopy of tektites, *Phys. Chem. Miner.*, *26*(6), 530–538, doi:10.1007/s002690050216.

Rossano, S., H. Behrens, and M. Wilke (2008), Advanced analyses of ^{57}Fe Mössbauer data of alumino-silicate glasses, *Phys. Chem. Miner.*, *35*(2), 77–93, doi:10.1007/s00269-007-0200-8.

Rossman, G. R., and M. N. Taran (2001), Spectroscopic standards for four-and fivefold-coordinated Fe^{2+} in oxygen-based minerals, *Am. Mineral.*, *86*(7–8), 896–903, doi:10.2138/am-2001-0713.

Seifert, F., and M. Olesch (1977), Mössbauer spectroscopy of grandidierite, (Mg, Fe)Al_3SiO_9, *Am. Mineral.*, *62*, 547–553.

Sturhahn, W. (2000), CONUSS and PHOENIX: Evaluation of nuclear resonant scattering data, *Hyperfine Interact.*, *125*(1–4), 149–172, doi:10.1088/0953-8984/16/5/009.

Thomas, C. W., Q. Liu, C. B. Agee, P. D. Asimow, and R. A. Lange (2012), Multi-technique equation of state for Fe_2SiO_4 melt and the density of Fe-bearing silicate melts from 0 to 161 GPa, *J. Geophys. Res.*, *117*, B10206, doi:10.1029/2012JB009403.

Toellner, T. S. (2000), Monochromatization of synchrotron radiation for nuclear resonant scattering experiments, *Hyperfine Interact.*, *125*(1–4), 3–28, doi:10.1023/A:1012621317798.

Victor, G. Y. V., D. Ghosh, and S. Ghose (2001), Ligand-field splitting of Fe^{2+} in distorted octahedral sites of the magnesium-rich orthopyroxenes $Fe_xMg_{1-x}SiO_3$: Correlation of magnetic susceptibility, Mössbauer, and optical absorption spectra, *Phys. Rev. B*, *64*(14), 144413, doi:10.1103/PhysRevB.64.144413.

Vidale, J. E., and M. A. Hedlin (1998), Evidence for partial melt at the core–mantle boundary north of Tonga from the strong scattering of seismic waves, *Nature*, *391*(6668), 682–685, doi:10.1038/35601.

Wilke, M., G. M. Partzsch, R. Bernhardt, and D. Lattard (2005), Determination of the iron oxidation state in basaltic glasses using XANES at the K-edge, *Chem. Geol.*, *220*(1–2), 143–161, doi:10.1016/j.chemgeo.2005.03.004.

Wilke, M., F. Farges, G. M. Partzsch, C. Schmidt, and H. Behrens (2007), Speciation of Fe in silicate glasses and melts by in-situ XANES spectroscopy, *Am. Mineral.*, *9*(1), 44–56, doi:10.2138/am.2007.1976.

Williams, Q., and E. J. Garnero (1996), Seismic evidence for partial melt at the base of Earth's mantle, *Science*, *273*(5281), 1528–1530, doi:10.1126/science.273.5281.1528.

Zhang, D., J. M. Jackson, W. Sturhahn, and Y. Xiao (2011), Local structure variations observed in orthoenstatite at high pressures, *Am. Mineral.*, *96*(10), 1585–1592, doi:10.2138/am.2011.3721.

Zhang, D., J. M. Jackson, J. Zhao, W. Sturhahn, E. E. Alp, T. S. Toellner, and M. Y. Hu (2015), Fast temperature spectrometer for samples under extreme conditions, *Rev. Sci. Instrum.*, *86*(1), 013105, doi:10.1063/1.4905431.

Zhe, L., T. Laixi, L. Xiaohan, R. Liudong, J. Mingzhi, and L. Milan (2000), Quadrupole splitting distributions in grandidierite and kornerupine from Antarctica, *Hyperfine Interact.*, *131*(1–4), 91–102, doi:10.1023/A:1010901706882.